Sensors & Actuators: B. Chemical 312 (2020) 127980

Contents lists available at ScienceDirect

Sensors and Actuators B: Chemical

journal homepage: www.elsevier.com/locate/snb

Label-free electrochemical immunosensor with palladium nanoparticles functionalized MoS_2/NiCo heterostructures for sensitive procalcitonin detection

Hui Ding[a], Lei Yang[a], Hongying Jia[a], Dawei Fan[a], Yong Zhang[a], Xu Sun[a], Qin Wei[a], Huangxian Ju[a,b,*]

[a] Collaborative Innovation Center for Green Chemical Manufacturing and Accurate Detection, Key Laboratory of Interfacial Reaction & Sensing Analysis in Universities of Shandong, School of Chemistry and Chemical Engineering, University of Jinan, Jinan 250022, PR China
[b] State Key Laboratory of Analytical Chemistry for Life Science, College of Chemistry and Chemical Engineering, Nanjing University, Nanjing 210023, PR China

ARTICLE INFO

Keywords:
Label-free electrochemical immunosensor
MoS_2/NiCo heterostructures
Pd NPs@MoS_2/NiCo
Procalcitonin
Signal amplification

ABSTRACT

An ultrasensitive label-free electrochemical immunosensor using MoS_2/NiCo heterostructures as an efficient signal enhancer was proposed for sensitive detection of procalcitonin. The MoS_2/NiCo heterostructures were synthesized by thermally depositing MoS_2 on NiCo MOFs nanocubes, which were then functionalized with in situ grown palladium nanoparticles (Pd NPs) for electrochemically catalyze the reduction of hydrogen peroxide. The presence of MoS_2/NiCo heterostructures greatly enhanced the electrocatalytic activity of Pd NPs, thus the Pd NPs@MoS_2/NiCo modified electrode showed amplified response to hydrogen peroxide. The large specific surface of Pd NPs@MoS_2/NiCo greatly improved the loading of antibody for preparation of immunosensor. Upon the incubation of the immunosensor with target procalcitonin, the electron transfer impendence increased, and thus the chronoamperometric response decreased, leading to a highly sensitive immunosensing method for detection of procalcitonin. The proposed method showed a linear range of 0.001–50 ng/mL with a detection limit of 0.36 pg/mL (S/N = 3). It possessed excellent accuracy and good practicality for diagnostics of PCT related diseases, and could be extended for development of other immunosensors for biomarkers detection.

1. Introduction

Sepsis refers to a systemic inflammatory response syndrome caused by maladjusted responses to infection [1,2], which has become the dominant reason of mortality for those seriously diseases [3]. Procalcitonin (PCT), the peptide precursor of the hormones [4], is a key biomarker in the diagnosis and detection of bacterial inflammation, which can reduce the misuse of antibiotic in serious patients [5]. Nowadays, with the rapid development of analytical and detection technologies, numerous efforts have been dedicated to the detection of PCT, including enzyme-linked immunosorbent assay (ELISA) [6], time-resolved digital immunoassay [7], microfluidic technology [8] and electrochemical biosensors [9]. Among these methods, electrochemical immunosensors based on distinctive antigen-antibody interaction [10] have received remarkable attention due to its low sample consumption, short analysis time and high sensitivity [11]. Considering that the sensitive detection of PCT in human serum is still a significant subject, effective efforts are still urgently demanded to be devoted into fabricating a highly efficient label-free electrochemical immunosensor for PCT detection with high sensitivity.

Metal-organic frameworks (MOFs), as emerging porous organic-inorganic hybrids, have drawn considerable attention with widespread applications in catalysis, drug delivery [12] and chemical sensors [13]. Typically, different functions of MOFs can be achieved through the incorporation of Fe, Co and Ni-based transition metal salts. Furthermore, MOFs are often utilized as precursors or templates for the synthesis of carbon-based materials, sulfides and phosphides due to their unique structural and electrochemical properties [14,15]. In view of the integrity crystal structures, uniform cubic morphologies, low agglomeration and high surface area of NiCo MOFs, this work prepared the molybdenum disulfide (MoS_2)/NiCo heterostructures to enhance the catalytic activity of palladium nanoparticles (Pd NPs) toward the reduction of hydrogen peroxide (H_2O_2) for the construction of highly sensitive immunosensors.

* Corresponding author at: Collaborative Innovation Center for Green Chemical Manufacturing and Accurate Detection, Key Laboratory of Interfacial Reaction & Sensing Analysis in Universities of Shandong, School of Chemistry and Chemical Engineering, University of Jinan, Jinan 250022, PR China.
E-mail address: hxju@nju.edu.cn (H. Ju).

https://doi.org/10.1016/j.snb.2020.127980
Received 31 December 2019; Received in revised form 3 March 2020; Accepted 10 March 2020
Available online 12 March 2020
0925-4005/

MoS_2 with excellent electronic properties and unique structures has been extensively studied in electrochemical filed as the typical representative of transition metal dichalcogenides [16,17]. The similarity between the sulfur edge of the MoS_2 structure and Pt-group catalysts in the free energy of atomic hydrogen bonding makes MoS_2 an ideal candidate for the Pt-group catalysts synthesis [18]. Furthermore, MoS_2 nanosheets exhibit high catalytic capacity toward H_2O_2 reduction [19]. Previous work demonstrated that the exchange current density of MoS_2 can be increased by incorporating transition metal atoms [20]. Crystalline analysis of MoS_2 nanosheets and cubic NiCo MOFs demonstrated the well-matched lattice spacing between the (220) lattice of NiCo MOFs and (104) lattice of MoS_2 [21,22], which might be beneficial to the fabrication of MoS_2/NiCo heterostructures [23]. Moreover, MoS_2/NiCo heterostructures possess large specific surface to facilitate the provision of more active sites. Therefore, the in situ growth of Pd NPs on the surface of MoS_2/NiCo heterostructures can not only enhance the catalytic performance, but also bind tightly antibody via strong Pd-N interaction.

Here, the designed Pd NPs@MoS_2/NiCo heterostructures efficiently increased the surface area for loading of antibody, and showed strong electrocatalytic ability for the reduction of H_2O_2, which remarkably improved the sensitivity of the immunosensor for detection of the antibody-related target. Using PCT as the target analyte, the developed amperometric immunoassay method exhibited good linearity over the PCT concentration from 0.001 to 50 ng/mL with a detection limit of 0.36 pg/mL (S/N = 3). The excellent performance of the immunosensor for sample detection and its simple preparation indicated its potential application in diagnostics of PCT related diseases. The proposed immunosensing strategy could be extended to the development of other immunosensors for biomarkers detection.

2. Experimental section

2.1. Materials and apparatus

PCT antibody and antigen were purchased from GenScript Biotech Corporation (Nanjing, China). Bovine serum albumin (BSA, 96–99 %) was gotten from Sigma reagent Co., Ltd. (St. Louis, MO, USA). All electrochemical tests were carried on CHI760E electrochemical workstation (Shanghai Chenhua Instrument Co., Ltd. China) conducted by a conventional three-electrode system with a modified glassy carbon electrode (GCE) as working, a saturated calomel electrode (SCE) as reference and a platinum electrode as counter electrodes. The details of other materials and apparatus were provided in Supplementary Material (SM).

2.2. Synthesis of Pd NPs@MoS_2/NiCo heterostructures

The preparation of Pd NPs@MoS_2/NiCo heterostructures was shown in Scheme 1A. Uniform NiCo MOFs nanocubes were firstly prepared by mixing 20 mL solution containing 0.174 g $Ni(NO_3)_2{\cdot}6H_2O$ and 0.263 g $C_6H_5Na_3O_7{\cdot}2H_2O$ in 20 mL solution of 6.65 mg/mL $K_3[Co(CN)_6]$ under stirring for 5 min [24]. After the mixture was aged in the dark for 21 h, the product was filtered, washed with water and alcohol and dried at 70 °C overnight to obtain NiCo MOFs nanocubes. The MoS_2/NiCo heterostructures were then synthesized according to the former work [24] with a little modification. 10 mg of $(NH_4)_2MoS_4$ and 30 mg of NiCo MOFs nanocubes were resolved in 30 mL of DMF under ultrasonication for 25 min. The DMF solution was transferred into a 50 mL Teflon-lined stainless steel autoclave to heat at 210 °C for 20 h. After cooled down, the mixture was centrifuged at 9000 rmp for 6 min to obtain the precipitation, which was washed with ethanol and water for five times and then dried at 70 °C overnight. MoS_2 was also synthesized as control in the same procedure in the absence of NiCo MOFs nanocubes.

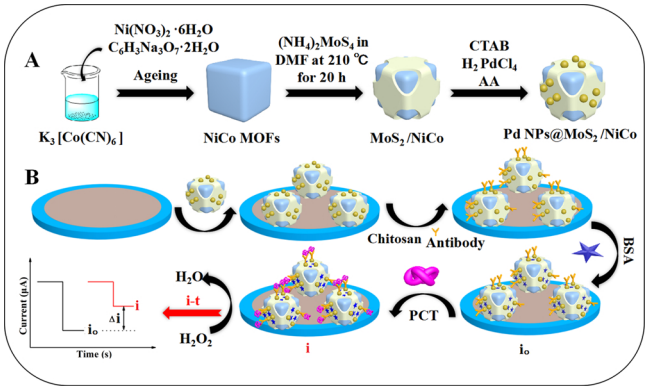

Scheme 1. (A) Illustration of the fabrication of Pd NPs@MoS_2/NiCo heterostructures and (B) the preparation of immunosensor as well as chronoamperometric detection of PCT.

2.0 mg of MoS_2/NiCo heterostructures was dispersed in 8 mL of aqueous solution containing 0.146 g of CTAB under ultrasonication. After centrifuged at 9000 rmp for 8 min and washed with water to remove extra CTAB, the heterostructures were redispersed in 10 mL of water, and mixed with 10 mL of H_2PdCl_4 with ultrasonication. 0.176 g of AA was then quickly added in the mixture to shake for 35 min. After the reaction mixture was put in dark for 6 h, the precipitation was filtered, washed with water and alcohol several times, and dried at 70 °C to obtain Pd NPs@MoS_2/NiCo heterostructures. Palladium nanoparticles functionalized NiCo MOFs (Pd NPs@NiCo) and palladium nanoparticles functionalized MoS_2 (Pd NPs@MoS_2) were also synthesized in the same procedure without the existence of MoS_2 or NiCo MOFs.

2.3. Construction of the immunosensor

The label-free sensing platform was prepared with stepwise assembly as shown in Scheme 1B. First of all, the bare GCE was polished with aluminum oxide powder and washed with water. The solution of Pd NPs@MoS_2/NiCo heterostructures (2.0 mg/mL, 6.0 μL) was then dropped onto the electrode and dried at room temperature. Next, chitosan solution (0.1 wt%, 4.0 μL) was added on the surface to immobilize the heterostructures on electrode. After drying, PCT antibody (10 μg/mL, 6.0 μL) was incubated on the GCE at 4 °C for 1 h. Afterwards, BSA (1 wt%, 3.0 μL) was added on the surface to block the nonspecific binding sites. The obtained immunosensor was stored at 4 °C for the following experiments.

2.4. Electrochemical measurements

The steady chronoamperometric response i_o of the immunosensor was firstly measured in PBS (0.07 mol/L, pH 7.38) at -0.1 V upon addition of 5.0 mmol/L H_2O_2. After 6.0 μL of PCT sample was dropped on immunosensor to incubate for 1 h, the chronoamperometric response i was recorded in PBS (0.07 mol/L, pH 7.38) at -0.1 V upon addition of 5.0 mmol/L H_2O_2 after the background current reached steady.

3. Results and discussion

3.1. Characterization of structure and morphology

Scanning electron microscope (SEM), transmission electron microscope (TEM) and X-ray diffraction (XRD) are powerful tools to prove the heterostructures. The obtained NiCo MOFs showed a shape

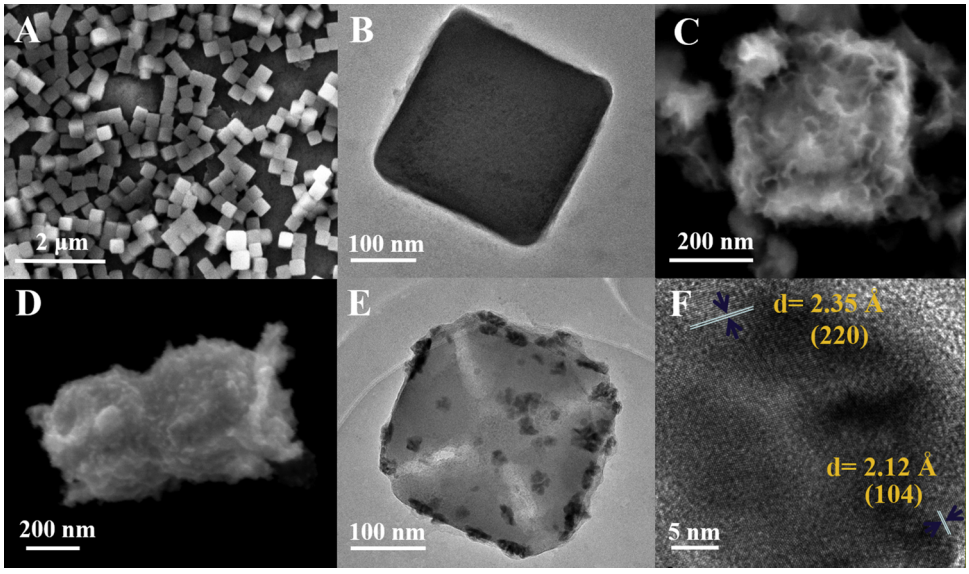

Fig. 1. (A) SEM and (B) TEM images of NiCo MOFs. SEM images of (C) MoS_2/NiCo and (D) Pd NPs@MoS_2/NiCo. (E) TEM image of Pd NPs@MoS_2/NiCo. (F) HRTEM image of MoS_2/NiCo.

of nanocube (Fig. 1A) with a size about 250 nm (Fig. 1B). After the MoS_2 nanosheets were thermally grown on NiCo MOFs, the product maintained the cubic structure and the size increased to about 260 nm (Fig. 1C). Furthermore, the surface of NiCo MOFs exhibited the ultrathin MoS_2 nanosheets, which led to obvious surface defects made the surface more rough. The reduction deposition of Pd NPs on the surface of MoS_2/NiCo heterostructures further increased the size to 270 nm (Fig. 1D), which showed the presence of Pd NPs on the cubic heterostructures (Fig. 1E). The MoS_2/NiCo heterostructures demonstrated the 0.235 nm lattice spacing of NiCo MOFs (220) and 0.212 nm lattice spacing of the MoS_2 (104) (Fig. 1F), indicating the well-matched lattice. Similarly, the element composition of the Pd NPs@MoS_2/NiCo heterostructures was confirmed by elemental mapping (Fig. S1), which indicated the even distribution of the Mo, S, Pd, Ni and Co elements and adequately demonstrated the formation of Pd NPs@MoS_2/NiCo heterostructures.

As control, Pd NPs@NiCo and Pd NPs@MoS_2 were also synthesized. Their SEM images shown the attachment of Pd NPs on the surface of NiCo MOFs and MoS_2 upon the in situ growth at room temperature (Fig. S2). The XRD patterns of NiCo MOFs and MoS_2/NiCo further verified their crystal structures (Fig. S3). The XRD spectrum of NiCo MOFs matched well with pure cubic $Ni_3[Co(CN)_6]_2$ (JCPDS no. 89-3738), while the peaks of MoS_2/NiCo located between the diffraction peaks of MoS_2 (JCPDS no. 17-0744) and cubic $Ni_3[Co(CN)_6]_2$.

In order to demonstrate the high specific surface of MoS_2/NiCo heterostructures, the nitrogen absorption-desorption isotherm was measured (Fig. 2A), which showed a calculated specific surface area of approximate 57.08 m^2/g. The relatively large specific surface area increased the active sites and provided favorable conditions for the loading of antibody.

The X-ray photoelectron spectroscopy (XPS) can provide further information about the surface composition and chemical bonding state. The presence of charge increased the binding energy, so the whole spectrum was corrected by C 1s binding energy (284.5 eV). The XPS survey spectrum of MoS_2/NiCo heterostructures demonstrated the high-resolution spectrum of Ni, Co, Mo and S elements (Fig. 2B). In the high resolution of Ni 2p spectrum (Fig. 2C), the fitting peaks at 856.1 eV and 873.7 eV were corresponding to Ni $2p_{3/2}$ and Ni $2p_{1/2}$ spin orbits, respectively. Moreover, the other two peaks at 862.3 eV and 879.8 eV were regarded as shake-up satellites of Ni $2p_{3/2}$ and Ni $2p_{1/2}$ [25], respectively. These results confirmed that nickel ions were mainly existed in the form of Ni^{2+} in the heterostructures. In the high-resolution XPS of Co 2p, four peaks ranging from 771.3 eV to 812.3 eV were observed (Fig. 2D). The peaks at 781.5 eV and 797.1 eV were assigned to Co $2p_{3/2}$ and Co $2p_{1/2}$, while the other two peaks at 786.5 eV and 803.5 eV belonged to shake-up satellites. The Mo 3d spectra revealed a mixture of Mo oxidation states (Fig. 2E). The binding energy at 235.2 eV could be related to Mo^{VI} $3d_{5/2}$, demonstrating the existence of amorphous MoS_3 [26]. The Mo^{V} $3d_{3/2}$ and Mo^{V} $3d_{5/2}$ at 232.2 eV and 229.3 eV with the separation energy approach to 2.9 eV resulted from Mo^{5+} ions [27]. The fitting peaks at 231.8 eV and 228.6 eV pointed to Mo^{IV} $3d_{3/2}$ and Mo^{IV} $3d_{5/2}$ spin orbits. Deserved to mentioned, the peak at 226.9 eV indexed as bridging disulfides (S_2^{2-}) [28]. The parameters of S_2^{2-} were thoroughly proved in the S 2p spectra (Fig. 2F). The single doublet at 161.8 eV proved that the S element existed as apical S^{2-} and the peak at 162.8 eV should be attributed to the S $2p_{1/2}$ orbitals [29]. The spectra became broaden at high binding energies, which could be ascribed to the formation of a small amount of NiS during the reaction progress, and NiS had conductivity at room temperature [30]. Furthermore, a significant peak at 168.4 eV could be on account of the oxidation reaction of metal sulfide on the surface [31]. In conclusion, the morphologic structures observed in SEM, TEM and XRD measurements and the surface compositions and binding energies suggested that the Pd NPs@MoS_2/NiCo heterostructures were well synthesized.

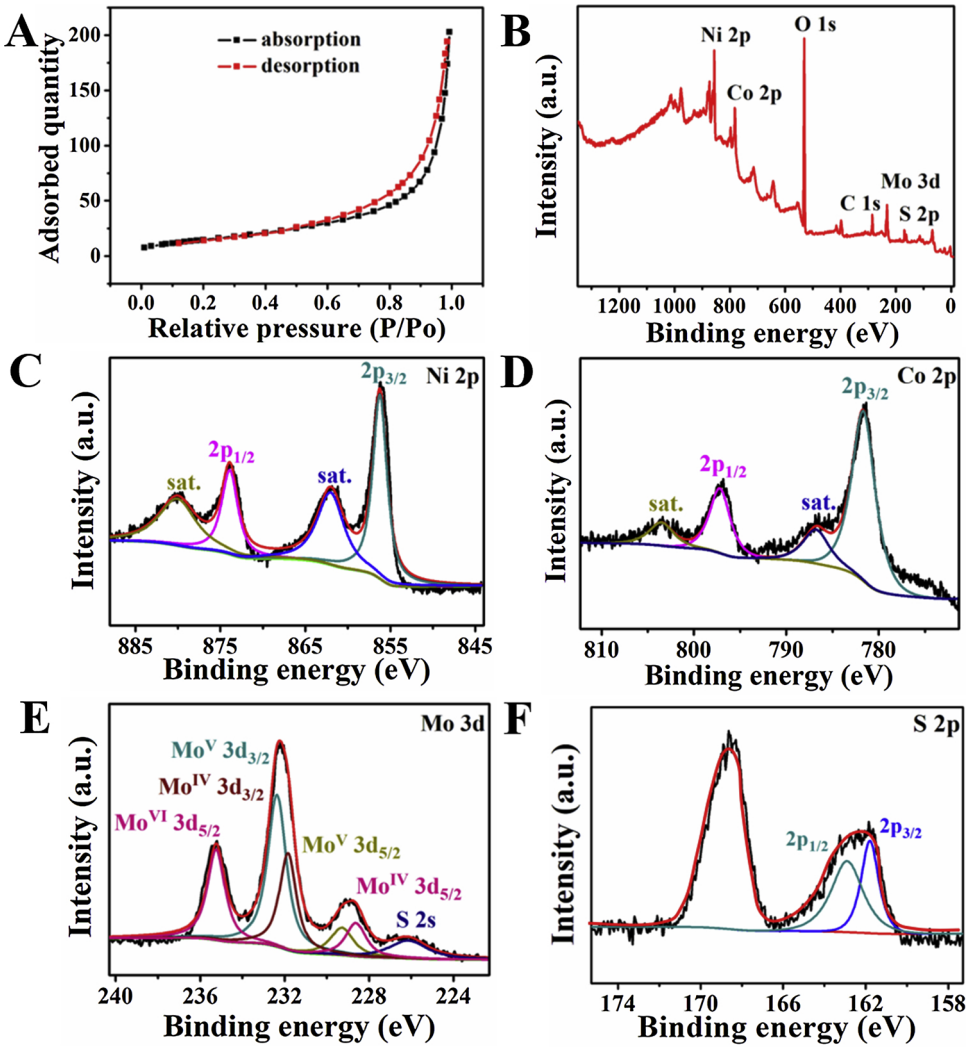

Fig. 2. (A) Nitrogen absorption-desorption isotherm of MoS_2/NiCo. (B) XPS survey spectrum of MoS_2/NiCo. High resolution spectra of (C) Ni 2p, (D) Co 2p, (E) Mo 3d and (F) S 2p.

3.2. Amplified amperometric response of the modified electrodes

Electrochemical characteristics of Pd NPs@MoS_2/NiCo heterostructures were performed with chronoamperometry and cyclic voltammetry (CV). As control, NiCo MOFs nanocubes, MoS_2/NiCo heterostructures, Pd NPs@NiCo, Pd NPs@MoS_2 and Pd NPs@MoS_2/NiCo heterostructures with the same amount (2.0 mg/mL, 6.0 μL) were coated on bare GCEs, respectively. The chronoamperometric curves were firstly recorded at the applied potential of -0.1 V in PBS (0.07 mol/L, pH 7.38) upon three additions of 0.015 mol/L H_2O_2 after the background reached steady. As shown in Fig. 3A, the response of NiCo MOFs modified GCE was almost zero (curve a), suggesting that NiCo MOFs could not catalyze the H_2O_2 reduction. However, the MoS_2/NiCo heterostructures and Pd NPs@NiCo modified GCEs showed weak current response upon three addition of 0.015 mol/L H_2O_2 (curves b and c), indicating their catalytic activity towards H_2O_2 reduction. Compared with Pd NPs@MoS_2 modified GCE, their catalytic activity were much weaker, and Pd NPs@MoS_2 modified GCE showed obviously enhanced amperometric response (curve d), indicating the synergy of Pd NPs and MoS_2 nanosheets toward the electrocatalytic reduction of H_2O_2. Interestingly, the response of Pd NPs@MoS_2/NiCo heterostructures modified electrode to H_2O_2 further increased (curve e), indicating the outstanding catalytic activity of Pd NPs@MoS_2/NiCo, which could be attributed to the large specific surface area of MoS_2/NiCo heterostructures for providing more active sites and the synergistic effects between various metal sulfide phases (NiS_x, CoS_x, NiMoS,and CoMoS) and MoS_2 [32–34]. The amplified amperometric response demonstrated the feasibility to use the designed nanomaterial for preparation of highly sensitive immunosensors.

According to the previous reports [35,36], the electrocatalytic reduction mechanism of H_2O_2 at Pd NPs@MoS_2/NiCo heterostructures modified electrode could be summarized as follows:

$$H_2O_2 + e^- \rightarrow OH^{\cdot}_{ad} + OH^- \quad (1)$$

$$OH^{\cdot}_{ad} + e^- \rightarrow OH^- \quad (2)$$

$$2OH^- + 2H^+ \rightarrow 2H_2O \quad (3)$$

Here, the adsorption of $OH^{\cdot}_{ad}$ on the surface active sites of the synthesized heterostructures played an important role in the reduction progress. Thus the CV curve of Pd NPs@MoS_2/NiCo modified electrode in PBS solution (0.07 mol/L, pH 7.38) containing 5.0 mmol/L H_2O_2 showed good response (Fig. 3B).

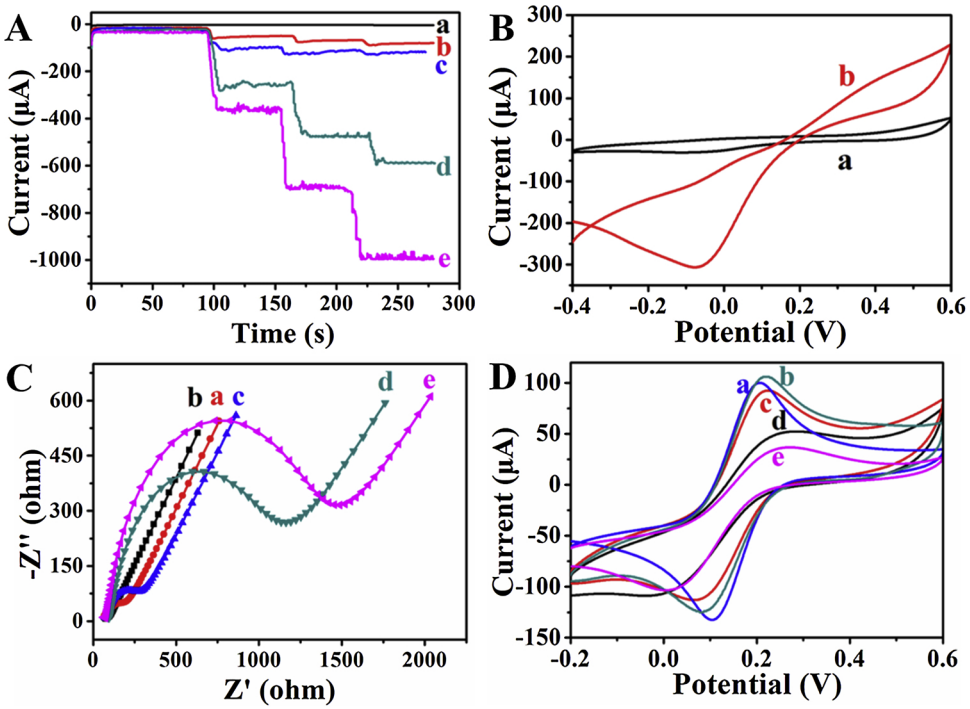

Fig. 3. (A) Chronoamperometric curves of (a) NiCo MOFs, (b) MoS_2/NiCo, (c) Pd NPs@NiCo, (d) Pd NPs@MoS_2 and (e) Pd NPs@MoS_2/NiCo modified electrodes at -0.1 V in PBS (0.07 mol/L, pH 7.38) upon three additions of 0.015 mol/L H_2O_2. (B) CV curves of Pd NPs@MoS_2/NiCo modified electrodes in 10 mL PBS (0.07 mol/L, pH 7.38) in (a) absence and (b) presence of 5.0 mmol/L H_2O_2. (C) EIS and (D) CV responses of (a) bare GCE, (b) Pd NPs@MoS_2/NiCo/GCE, (c) Ab/Pd NPs@MoS_2/NiCo/GCE, (d) BSA/Ab/Pd NPs@MoS_2/NiCo/GCE, (e) PCT/BSA/Ab/Pd NPs@MoS_2/NiCo/GCE in 0.10 mol/L KCl containing 5.0 mmol/L $[Fe(CN)_6]^{3-/4-}$ for EIS and 5.0 mmol/L $[Fe(CN)_6]^{3-}$ for CV.

3.3. Characterization of the immunosensor

A.C. impedance was used to evaluate the change of electron transfer rate during preparation of electrochemical immunosensors [37]. The Nyquist plot contains two parts: the linear portion at low frequencies is related to the diffusion-controlled electrochemical behavior, while the semicircle portion at high frequencies reflects the electron transfer rate or electron transfer resistance (R_{et}) [38]. The experiments were performed in 0.10 mol/L KCl solution containing 5.0 mmol/L $[Fe(CN)_6]^{3-/4-}$, and the frequency range was 10^{-1} Hz - 10^5 Hz. As shown in Fig. 3C, the bare GCE exhibited a small R_{et} (curve a). After Pd NPs@MoS_2/NiCo was coated on GCE, the Nyquist plot appeared an almost straight line (curve b), revealing that Pd NPs@MoS_2/NiCo owned great electron transfer ability. After anti-PCT antibody (Ab), BSA and PCT were assembled on the Pd NPs@MoS_2/NiCo modified GCE in sequence, the resistance increased gradually (curves c–e), which were caused by the nonconductive properties of biomolecule as the blocking layer. The cyclic voltammograms in 0.10 mol/L KCl solution containing 5.0 mmol/L $[Fe(CN)_6]^{3-}$ shown similar results (Fig. 3D). The redox peaks at Pd NPs@MoS_2/NiCo heterostructures modified electrode showed the maximum values. These phenomenon confirmed the successful construction of immunosensor for PCT.

3.4. Optimization of experimental conditions

The effects of pH value of PBS for electrochemical detection and concentration of Pd NPs@MoS_2/NiCo heterostructures used for immunosensor preparation on amperometric response were examined to obtain the optimal conditions. The pH value mainly affected the catalytic properties towards H_2O_2 reduction and altered the activity of proteins. The maximum response of the proposed immunosensor occurred at pH 7.38 (Fig. S4A), which was chosen for the whole experiments.

The amount of Pd NPs@MoS_2/NiCo heterostructures coated on electrode surface affected both the immobilization of Ab and the electrocatalytic process towards H_2O_2 reduction. With the increasing concentration of Pd NPs@MoS_2/NiCo heterostructures, the response of the immunosensor to PCT increased and then decreased at 2.0 mg/mL (Fig. S4B). The decreased response could be attributed to the hindered electron transfer due to the increasing film thickness. Therefore, 6.0 μL of 2.0 mg/mL of Pd NPs@MoS_2/NiCo heterostructures was chosen for immunosensor preparation.

3.5. Performance of the proposed immunosensor

The proposed label-free immunosensor was applied to detect PCT

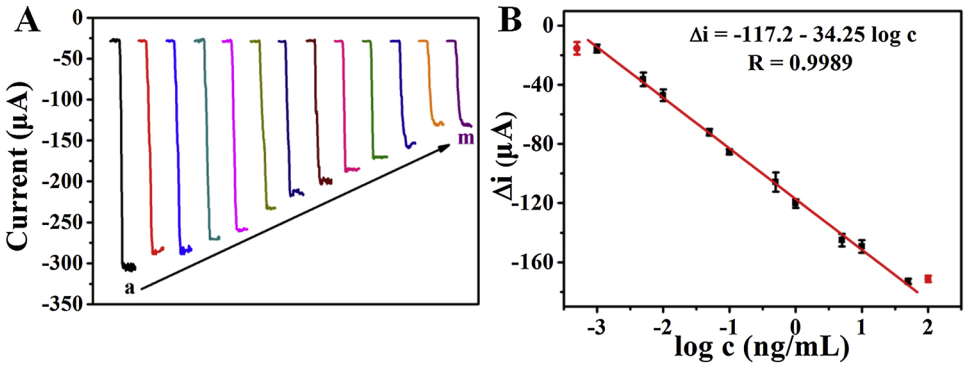

Fig. 4. (A) Chronoamperometric responses of immunosensor incubated with PCT at 0, 0.0005, 0.001, 0.005, 0.01, 0.05, 0.1, 0.5, 1, 5, 10, 50, 100 ng/mL (from a to m) in 10 mL PBS (0.07 mol/L, pH 7.38) upon addition of 5.0 mmol/L H_2O_2. (B) Plot of signal change (Δi) of the immunosensor upon incubation with PCT vs logarithm of PCT concentration (from 0.0005 to 100 ng/mL).

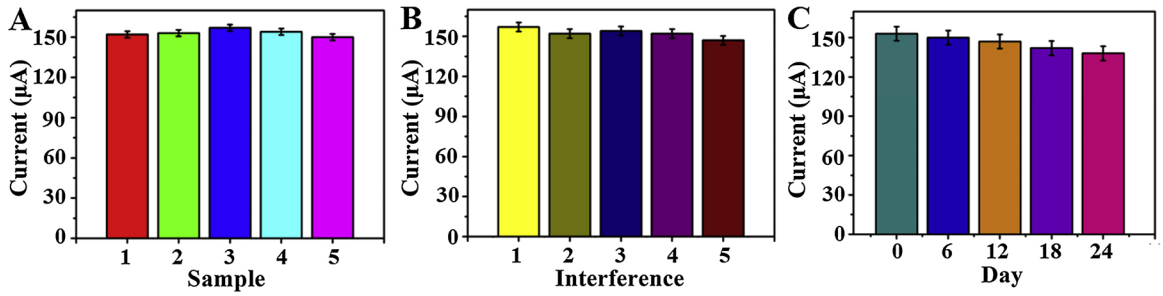

Fig. 5. (A) Reproducibility of the immunosensor at 1 ng/mL PCT. (B) Response of the immunosensor to 1 ng/mL PCT (1), and 1 ng/mL PCT +50 ng/mL PSA (2), 1 ng/mL PCT +50 ng/mL IgG (3), 1 ng/mL PCT +50 ng/mL AFP (4), 1 ng/mL PCT +50 ng/mL CEA (5). (C) Stability of the immunosensor at 1 ng/mL PCT. All the tests were performed in 10 mL PBS (0.07 mol/L, pH 7.38) containing 5.0 mmol/L H_2O_2 at potential of -0.1 V. The error bars were obtained from the standard deviation of five measurements.

concentration through chronoamperometry. With the increasing PCT concentration from 0 to 100 ng/mL (where 0 ng/mL was a blank), the chronoamperometric response of the PCT incubated immunosensor to 5.0 mmol/L H_2O_2 in 10 mL PBS (0.07 mol/L, pH 7.38) decreased (Fig. 4A). This was because more PCT were bound to immunosensor surface to increase both the electron transfer resistance and the steric resistance for access of H_2O_2. The plot of the signal change Δi ($\Delta i = i_o - i$) of the immunosensor vs the logarithm of PCT concentration from 0.001 to 50 ng/mL showed good linearity (Fig. 4B). The linear regression equation was $\Delta i = -117.2 - 34.25 \log c$ (ng/mL) with a correlation coefficient of 0.9989. The detection limit was calculated at 3 S/N to be 0.36 pg/mL. The high sensitivity of the label-free electrochemical immunosensor was ascribed to the amplified signal. Compared with the reported methods for PCT, the proposed immunosensor showed wider linear range (Table S1), which came from the large specific surface area for loading of antibody, which provided more binding sites for recognition of target PCT.

3.6. Reproducibility, selectivity and stability of the immunosensor

The reproducibility of immunosensors is one of the vital indexes for the widespread application. Five immunosensors were prepared to test the chronoamperometric response of 1.0 ng/mL of PCT, which showed the relative standard deviation (RSD) of 1.69 % (Fig. 5A), indicating that the constructed immunosensor possessed well-deserved reproducibility.

The specificity is a significant feature for immunosensor. Prostate specific antigen (PSA), immunoglobulin G (IgG), alpha fetoprotein (AFP) and carcinoembryonic antigen (CEA) were introduced as diverse interfering species (50 ng/mL) and mixed with 1.0 ng/mL of PCT to examine the specificity of the constructed immnunosensor. As illustrated in Fig. 5B, no obvious variation was caused by these interfering substances, and the RSD of the obtained signals was less than 5%, showing superior specificity of the proposed immunosensor.

After the immunosensors were stored at 4 °C for different days (Fig. 5C), they were used for detecting 1.0 ng/mL PCT. The current response maintained at 90% after 24 days, revealing that the stability was acceptable. It speculated that the durable stability was on account of the favorable biomolecular affinity of Pd NPs@MoS_2/NiCo heterostructures, ensuring the stability of antibody on the electrode surface.

3.7. Real sample analysis

To prove the reliability of the immunosensor in practical application, the recovery experiments were implemented by adding continuously PCT standard solution to human serum samples. As shown in Table S2, the recovery rates were changed within a range of 97.9 % ~ 103.6 %, and the RSD were from 1.24% to 2.27%, demonstrating that the constructed immunosensor was adequate for the PCT detection in serum samples.

4. Conclusion

This work designs Pd NPs@MoS_2/NiCo heterostructures for construction of label-free electrochemical immunosensor. The large specific surface area of MoS_2/NiCo heterostructures provides abundant active sites for deposition of Pd NPs. The coexistence of Pd NPs and MoS_2 shows effective synergy on the electrocatalytic reduction of H_2O_2. The MoS_2/NiCo heterostructures can act as the excellent signal enhancer for amplified immunosensing. Using PCT as the analyte model, the anti-PCT antibody can be conveniently adsorbed on Pd NPs@MoS_2/NiCo heterostructures modified electrode via strong Pd-N interaction. The high loading of antibody provides more binding sites for recognition of target PCT. The proposed immunosensor shows high sensitivity, low detection limit, wide detection range, and remarkable reproducibility, specificity and stability, and has been used for PCT detection in real serum samples. This amplified immunoassay demonstrates the good extendability of the heterostructures and the designed label-free immunosensing strategy for other biomarkers.

CRediT authorship contribution statement

Hui Ding: Conceptualization, Investigation, Data curation, Writing - original draft, Methodology. **Lei Yang:** Conceptualization, Investigation. **Hongying Jia:** Investigation. **Dawei Fan:** Project administration, Investigation. **Yong Zhang:** Investigation. **Xu Sun:** Investigation. **Qin Wei:** Project administration, Funding acquisition. **Huangxian Ju:** Conceptualization, Project administration, Funding acquisition, Writing - review & editing.

Declaration of Competing Interest

The authors declare that they have not known competing financial interests or personal relationships that could have appeared to influence the work reported in this paper.

Acknowledgements

This study was supported by the Special Foundation for Taishan Scholar Professorship of Shandong Province (No. ts201712052), the National Key Scientific Instrument and Equipment Development Project of China (No. 21627809), the National Natural Science Foundation of China (Nos. 21505051, 21575050, 21777056), and the Jinan Scientific Research Leader Workshop Project (2018GXRC024).

Appendix A. Supplementary data

Supplementary material related to this article can be found, in the online version, at doi:https://doi.org/10.1016/j.snb.2020.127980.

References

[1] H. Lee, Procalcitonin as a biomarker of infectious diseases FAU, Korean J. Intern. Med. 28 (2013) 285–291.
[2] L. Yang, D. Fan, Y. Zhang, C. Ding, D. Wu, Q. Wei, H. Ju, Ferritin-based electrochemiluminescence nanosurface energy transfer system for procalcitonin detection using HWRGWVC heptapeptide for site-oriented antibody immobilization, Anal. Chem. 91 (2019) 7145–7152.
[3] D.C. Angus, W.T. Linde-Zwirble, J. Lidicker, G. Clermont, J. Carcillo, M.R. Pinsky, Epidemiology of severe sepsis in the United States: analysis of incidence, outcome, and associated costs of care, Crit. Care Med. 29 (2001) 1303–1310.
[4] S.J. Wimalawansa, Amylin, calcitonin gene-related peptide, calcitonin, and adrenomedullin: a peptide superfamily, Crit. Rev. Neurobiol. 11 (1997) 167–239.
[5] M. Christ-Crain, D. Jaccard-Stolz, R. Bingisser, M.M. Gencay, P.R. Huber, M. Tamm, B. Müller, Effect of procalcitonin-guided treatment on antibiotic use and outcome in lower respiratory tract infections: cluster-randomised, single-blinded intervention trial, Lancet 363 (2004) 600–607.
[6] S.D. Gan, K.R. Patel, Enzyme immunoassay and enzyme-linked immunosorbent assay, J. Invest. Dermatol. 133 (2013) 1–3.
[7] W. Jing, Y. Wang, Y. Yang, Y. Wang, G. Ma, S. Wang, N. Tao, Time-resolved digital immunoassay for rapid and sensitive quantitation of procalcitonin with plasmonic imaging, ACS Nano 13 (2019) 8609–8617.
[8] R. Yang, J. Wang, Y. Gao, Advances of microfluidic technologies applied in diagnosis and treatment of sepsis, Zhongguo Wei Zhong Bing Ji Jiu Yi Xue 31 (2019) 789–792.
[9] Z.H. Yang, Y. Zhuo, R. Yuan, Y.Q. Chai, Electrochemical activity and electrocatalytic property of cobalt phthalocyanine nanoparticles-based immunosensor for sensitive detection of procalcitonin, Sens. Actuator B-Chem. 227 (2016) 212–219.
[10] J.H. Lin, H.X. Ju, Electrochemical and chemiluminescent immunosensors for tumor markers, Biosens. Bioelectron. 20 (2005) 1461–1470.
[11] H. Wang, Y. Zhang, Y.L. Wang, H.M. Ma, B. Du, Q. Wei, Facile synthesis of cuprous oxide nanowires decorated graphene oxide nanosheets nanocomposites and its application in label-free electrochemical immunosensor, Biosens. Bioelectron. 87 (2017) 745–751.
[12] Y. Li, R.T. Yang, Gas adsorption and storage in metal-organic framework MOF-177, Langmuir 23 (2007) 12937–12944.
[13] P. Falcaro, R. Ricco, C.M. Doherty, K. Liang, A.J. Hill, M.J. Styles, MOF positioning technology and device fabrication, Chem. Soc. Rev. 43 (2014) 5513–5560.
[14] X.L. Yan, X.J. Li, Z.F. Yan, S. Komarneni, Porous carbons prepared by direct carbonization of MOFs for supercapacitors, Appl. Surf. Sci. 308 (2014) 306–310.
[15] Z. Jiang, W.J. Lu, Z.P. Li, K.H. Ho, X. Li, X.L. Jiao, D.R. Chen, Synthesis of amorphous cobalt sulfide polyhedral nanocages for high performance supercapacitors, J. Mater. Chem. A. 2 (2014) 8603–8606.
[16] F.Y. Li, Y.Y. Li, J.H. Feng, Z.Q. Gao, H. Lv, X. Ren, Q. Wei, Facile synthesis of MoS_2@Cu_2O-Pt nanohybrid as enzyme-mimetic label for the detection of the hepatitis B surface antigen, Biosens. Bioelectron. 100 (2018) 512–518.
[17] Z.Q. Gao, Y.Y. Li, X.B. Zhang, J.H. Feng, L. Kong, P. Wang, Z.W. Chen, Y.H. Dong, Q. Wei, Ultrasensitive electrochemical immunosensor for quantitative detection of HBeAg using Au@Pd/MoS_2@MWCNTs nanocomposite as enzyme-mimetic labels, Biosens. Bioelectron. 102 (2018) 189–195.
[18] X.P. Ren, Q. Ma, H.B. Fan, L.Q. Pang, Y.X. Zhang, Y. Yao, X.D. Ren, S.Z. Liu, A Se-doped MoS_2 nanosheet for improved hydrogen evolution reaction, Chem. Commun. 51 (2015) 15997–16000.
[19] X. Wang, C.C. Chu, L. Shen, W.P. Deng, M. Yan, S.G. Ge, J.H. Yu, X.R. Song, An ultrasensitive electrochemical immunosensor based on the catalytical activity of MoS_2-Au composite using Ag nanospheres as labels, Sens. Actuator B-Chem. 206 (2015) 30–36.
[20] H.T. Wang, C. Tsai, D.S. Kong, K.R. Chan, F. Abild-Pedersen, J. Norskov, Y. Cui, Transition-metal doped edge sites in vertically aligned MoS_2 catalysts for enhanced hydrogen evolution, Nano Res. 8 (2015) 566–575.
[21] N. Ma, T. Zhang, D.W. Fan, X. Kuang, A. Ali, D. Wu, Q. Wei, Triple amplified ultrasensitive electrochemical immunosensor for alpha fetoprotein detection based on MoS_2@Cu_2O-Au nanoparticles, Sens. Actuator B-Chem. 297 (2019) 8.
[22] Q.F. Wang, B. Liu, X.F. Wang, S.H. Ran, L.M. Wang, D. Chen, G.Z. Shen, Morphology evolution of urchin-like $NiCo_2O_4$ nanostructures and their applications as psuedocapacitors and photoelectrochemical cells, J. Mater. Chem. 22 (2012) 21647–21653.
[23] L. Yang, Y. Jia, D. Wu, Y. Zhang, H.X. Ju, Y. Du, H.M. Ma, Q. Wei, Synthesis and application of CeO_2/SnS_2 heterostructures as a highly efficient coreaction accelerator in the luminol-dissolved O_2 system for ultrasensitive biomarkers immunoassay, Anal. Chem. 91 (2019) 14066–14073.
[24] X.Y. Yu, Y. Feng, Y. Jeon, B. Guan, X.W. Lou, U. Paik, Formation of Ni-Co-MoS_2 nanoboxes with enhanced electrocatalytic activity for hydrogen evolution, Adv. Mater. 28 (2016) 9006–9011.
[25] L. Peng, X. Ji, H.Z. Wan, Y.J. Ruan, K. Xu, C. Chen, L. Miao, J.J. Jiang, Nickel sulfide nanoparticles synthesized by microwave-assisted method as promising supercapacitor electrodes: an experimental and computational study, Electrochim. Acta 182 (2015) 361–367.
[26] J.D. Benck, Z. Chen, L.Y. Kuritzky, A.J. Forman, T.F. Jaramillo, Amorphous molybdenum sulfide catalysts for electrochemical hydrogen production: insights into the origin of their catalytic activity, ACS Catal. 2 (2012) 1916–1923.
[27] H. Vrubel, D. Merki, X. Hu, Hydrogen evolution catalyzed by MoS_3 and MoS_2 particles, Energy Environ. Sci. 5 (2012) 6136–6144.
[28] J. Bonde, P.G. Moses, T.F. Jaramillo, J.K. Norskov, I. Chorkendorff, Hydrogen evolution on nano-particulate transition metal sulfides, Faraday Discuss. 140 (2008) 219–231.
[29] W. Xing, F. Li, Z.F. Yan, G.Q. Lu, Synthesis and electrochemical properties of mesoporous nickel oxide, J. Power Sources 134 (2004) 324–330.
[30] P.H. Citrin, High-resolution X-ray photoemission from sodium metal and its hydroxide, Phys. Rev. B 8 (1973) 5545–5556.
[31] J.C. Xing, Y.L. Zhu, Q.W. Zhou, X.D. Zheng, Q.J. Jiao, Fabrication and shape evolution of CoS_2 octahedrons for application in supercapacitors, Electrochim. Acta 136 (2014) 550–556.
[32] H. Zhang, Y. Li, T. Xu, J. Wang, Z. Huo, P. Wan, X. Sun, Amorphous Co-doped MoS_2 nanosheet coated metallic CoS_2 nanocubes as an excellent electrocatalyst for hydrogen evolution, J. Mater. Chem. A. 3 (2015) 15020–15023.
[33] X.P. Dai, K.L. Du, Z.Z. Li, M.Z. Liu, Y.D. Ma, H. Sun, X. Zhang, Y. Yang, Co-doped MoS_2 nanosheets with the dominant CoMoS phase coated on carbon as an excellent electrocatalyst for hydrogen evolution, ACS Appl. Mater. Interfaces 7 (2015) 27242–27253.
[34] D.Z. Wang, X.Y. Zhang, Y.L. Shen, Z.Z. Wu, Ni-doped MoS_2 nanoparticles as highly active hydrogen evolution electrocatalysts, RSC Adv. 6 (2016) 16656–16661.
[35] G. Flatgen, S. Wasle, M. Lubke, C. Eickes, G. Radhakrishnan, K. Doblhofer, G. Ertl, Autocatalytic mechanism of H_2O_2 reduction on Ag electrodes in acidic electrolyte: experiments and simulations, Electrochim. Acta 44 (1999) 4499–4506.
[36] H. Wei, E.K. Wang, Nanomaterials with enzyme-like characteristics (nanozymes): next-generation artificial enzymes, Chem. Soc. Rev. 42 (2013) 6060–6093.
[37] Y.G. Wang, G.H. Zhao, H. Wang, W. Cao, B. Du, Q. Wei, Sandwich-type electrochemical immunoassay based on Co_3O_4@MnO_2-thionine and pseudo-ELISA method toward sensitive detection of alpha fetoprotein, Biosens. Bioelectron. 106 (2018) 179–185.
[38] B. Kavosi, A. Salimi, R. Hallaj, F. Moradi, Ultrasensitive electrochemical immunosensor for PSA biomarker detection in prostate cancer cells using gold nanoparticles/PAMAM dendrimer loaded with enzyme linked aptamer as integrated triple signal amplification strategy, Biosens. Bioelectron. 74 (2015) 915–923.

Hui Ding studies in School of Chemistry and Chemical Engineering, University of Jinan as a postgraduate student.

Lei Yang studies in School of Chemistry and Chemical Engineering, University of Jinan as a doctoral student.

Hongying Jia studies in School of Chemistry and Chemical Engineering, University of Jinan as a doctoral student.

Dawei Fan received her Ph. D degree from Lanzhou Institute of Chemical Physics, Chinese Academy of Sciences, and is currently an associate professor at University of Jinan. Her main research interests focus on electrochemical and photoelectrochemical sensors. She has published over 50 articles in different journals

Yong Zhang received his B.S. degree in applied chemistry from University of Jinan in 2001, M.S. degree in applied chemistry from Nanjing University of Technology in 2005 and Ph.D. degree in Beijing Institute of Technology in 2016. He is currently an associate professor at University of Jinan. His main research interests focus on chemical sensors and biosensors.

Xu Sun received her Ph.D. in inorganic chemistry at University of Science and Technology of China (USTC). She is now working as an associate professor in School of Chemistry and Chemical Engineering in University of Jinan. Her research interests focus on the design and fabrication of novel nanomaterials for the construction of energy-related devices.

Qin Wei is a professor at University of Jinan. Her main research interests include the determination of proteins and nucleic acids. She has published over 100 articles.

Huangxian Ju received his BS, MS and Ph.D. degrees from Nanjing University during 1982–1992. He was a postdoc in Montreal University (Canada) in 1996–1997. He became an associate and full professor of Nanjing University in 1993 and 1999. He is currently the director of State Key Laboratory of Analytical Chemistry for Life Science. His research interests focus on analytical biochemistry, biosensing and molecular diagnosis. He has published 690 papers in different journals with h-index of 91 (Google Scholar h-index 100 with 35298 citations).